ACCELERATING LAGRANGIAN FLUID SIMULATION WITH GRAPH NEURAL NETWORKS

Zijie Li
Department of Mechanical Engineering
Carnegie Mellon University
Pittsburgh, PA 15213
zijieli@andrew.cmu.edu

Amir Barati Farimani
Department of Mechanical Engineering
Carnegie Mellon University
Pittsburgh, PA 15213
barati@cmu.edu

ABSTRACT

We present a data-driven model for fluid simulation under Lagrangian representation. Our model uses graphs to describe the fluid field, where physical quantities are encoded as the node and edge features. Instead of directly predicting the acceleration or position correction given the current state, we decompose the simulation scheme into separate parts - advection, collision, and pressure projection. For these different reasoning tasks, we propose two kinds of graph neural network structures, node-focused networks, and edge-focused networks. By introducing physics prior knowledge, computational costs in the training and inference stage are significantly reduced. Our tests show that the learned model can produce accurate results and remain stable in scenarios with a large number of particles and different geometries. Unlike many other data-driven models, further tests demonstrate that our model is able to retain many important physical properties of incompressible fluids, such as minor divergence and reasonable pressure distribution. Additionally, our model can adopt a range of time step sizes different from ones using in the training set, which indicates its robust generalization capability.

1 INTRODUCTION

For many science and engineering problems, fluids are an essential integral part. How to simulate fluid dynamics accurately has long been studied by researchers and a large class of numerical models have been developed. However, computing high-quality fluid simulation is still computationally expensive despite the advances in computing power. Also, the time of calculation usually increases drastically when the resolution of the simulating scene scales up. A common way to alleviate computing costs is to use reduced-order models. Recent progress in the machine learning domain opens up the possibility of employing learning algorithms to learn and predict fluid dynamics in an efficient way.

In this paper, we propose a graph-based data-driven fluid dynamics model, Fluid Graph Networks (FGN), which consists of simple multi-layer perceptron (MLP) and graph inductive architectures. The proposed model can retain the physical properties of the system without direct supervision (i.e. without adding a loss term based on these metrics), like low velocity-divergence and constant particle density. It can also predict reasonable pressure distribution. Further experiments demonstrate that our model can remain stable and accurate in the long-term simulation of scenarios involving different geometries.

2 RELATED WORKS

Our model is built upon the Lagrangian representation of fluid, where continuous fluids are discretized and approximated by a set of particles. The most prominent advantage of the Lagrangian method is that the particle boundary is the material interface, which makes boundary conditions easy to impose, especially when the material interface is large and changing violently. A well-known Lagrangian method is Smooth Particle Hydrodynamics (SPH)(Monaghan, 1988). SPH and its variants are widely used in numerical physics simulation, including fluid dynamics under various conditions (Müller

et al., 2003; Koshizuka and Oka, 1996; Becker and Teschner, 2007; Solenthaler and Pajarola, 2009; Bender and Koschier, 2015).

High-fidelity simulation based on traditional methods usually demands very fine resolution at time and space, which is computationally expensive. Modeling fluid dynamics in a data-driven way has been explored as an attractive alternative. With advances in machine learning algorithms, many data-driven models employing machine learning algorithms have been built to improve the computational efficiency of fluid simulation (Ladický et al., 2015; Tompson et al., 2016; Xiao et al., 2020; Wiewel et al., 2018; Morton et al., 2018; de Avila Belbute-Peres et al., 2020).

The building blocks of this work are neural networks built upon graphs (Scarselli et al., 2009). Learning and reasoning particle dynamics under graph representation has the following benefits and conveniences. First, particle-based methods model physics phenomena as interactions between particles within a local area. This imposes an inductive bias for learning under the Lagrangian framework: dynamics have a strong locality. The locality of unstructured data under Lagrangian representation can be captured by message passing and aggregation process on graphs, such as GCN and other variants (Kipf and Welling, 2016; Hamilton et al., 2017). Second, unlike Eulerian grid-based methods, Lagrangian particle-based methods do not have an explicit and structured grid, which makes standard Convolutional Neural Network (CNN) cannot be directly applied to particles without feature processing (Wang et al., 2018; Ummenhofer et al., 2020). Third, many dynamics are based on pairwise relations between particles, like collision, which can be emulated by message passing via edges in graph neural networks. Given these factors, recently there have been a large array of works that use graph neural networks to learn and reason about the underlying physics of interacting objects and particles. (Battaglia et al., 2016; Chang et al., 2016; Sanchez-Gonzalez et al., 2018; Li et al., 2018; Mrowca et al., 2018)

3 MODEL

3.1 FLUID DYNAMICS

The governing equation for incompressible fluids is the Navier-Stokes equation and the continuity equation as follows (Batchelor, 2000):

$$\frac{D\mathbf{u}}{Dt} = -\frac{\nabla p}{\rho} + \nu\nabla^2\mathbf{u} + \mathbf{g}, \tag{1}$$

$$\nabla \cdot \mathbf{u} = 0. \tag{2}$$

Here, we adopt the Lagrangian framework to track and describe the fluids, and we discretize field function and operator following the convention in SPH (See appendix A.1 for the definition of SPH).

3.2 MODEL

Fluids are time-dependent dynamical systems, where location of particles, $\mathbf{r}$, is described by equation of form: $d\mathbf{r}/dt = f(\mathbf{r})$. Here we assume the system is Markovian, that is, the state of the system at time step $n+1$ depends only on the state of the previous time step n. The update mechanism in our model can be defined as:

$$\{\mathbf{x}^{n+1}, \mathbf{v}^{n+1}\} = G_\theta\left(\{\mathbf{x}^n, \mathbf{v}^n\}\right). \tag{3}$$

Here $\{\mathbf{x}^n, \mathbf{v}^n\}$ denotes the positional information and velocity of fluid field at time step n. Data-driven model G_θ, parameterized by θ , maps the state of time step n to time step $n+1$.

We propose two types of graph neural networks to emulate the different physical processes involved in fluid dynamics. They can be divided into two types of graph networks (GN) according to the network structure (Battaglia et al., 2018).

Node-focused Graph Network We use node-focused GN to predict advection and projection process in fluid simulation. Advection net is responsible for the prediction of advection effect and pressure net is responsible for pressure projection. Considering a particle i, the node-focused graph network first aggregates node features from neighbor particles $\{v_j|\forall j \in \mathcal{N}(i)\}$ and output node embedding $\mathbf{f}_i$. The embedding $\mathbf{f}_i$ will then be passed to a processor g_R, which will predict the

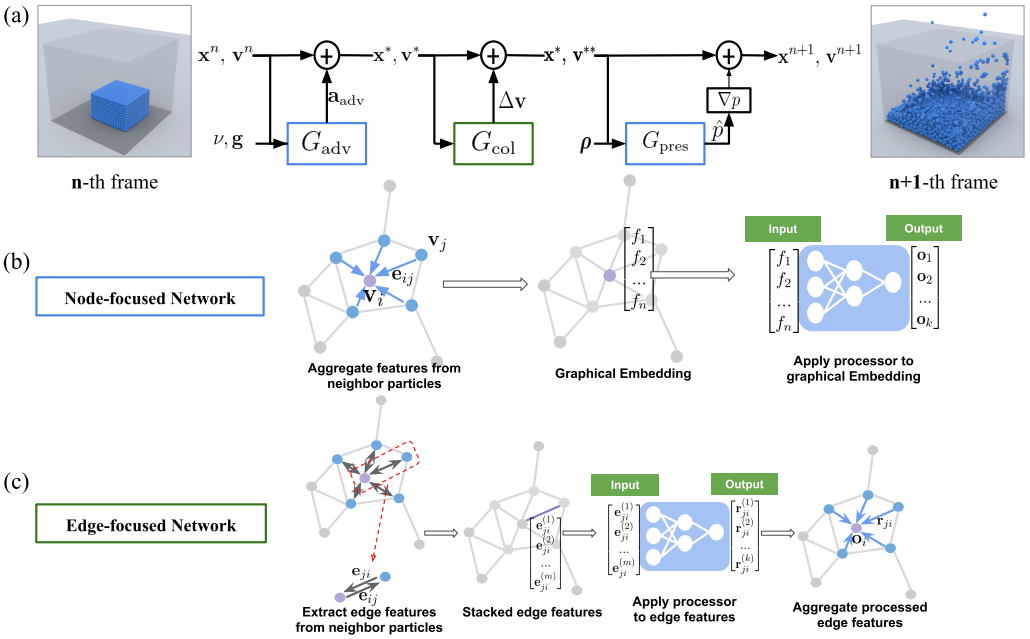

Figure 1: **(a)** Schematic of our FGN model. G_{adv} applies the effect of body force and viscosity to the fluids. G_{pres} predicts the pressure. G_{col} handles collision between particles. **(b)** In a node-focused network, input is represented as node features and then passed to a shared processor. **(c)** In an edge-focused network, input is represented as edge features of a directed graph, the edge features are then passed to a shared processor.

desirable physical quantities o_i (i.e. acceleration $\mathbf{a}$ in advection net and pressure p in pressure net). The whole message passing procedure can be defined as:

$$o_i = g_R\left(g_A\left(V_i\right)\right), V_i = \{v_j\}_{\forall j \in \mathcal{N}(i)}. \tag{4}$$

Edge-focused Graph Network We use edge-focused GN to drive away particles that are too close to each other, which emulates the elastic collision process. In collision net, relative features, e_{ij} (relative positions, relative velocities between particle i and j), are passed to processor f_R as edge features. These relative features impose spatial invariance on the model. The processor will output the edge embedding r_{ij} between each pair of nodes. Lastly, edge embedding r_{ij} is aggregated via aggregator f_A, to gather the influence from all nearby particles and predict an overall effect o_i on the center particle i. The message passing function in a layer of edge-focused graph network is defined as:

$$o_i = f_A\left(f_R\left(E_i\right)\right), E_i = \{e_{ij}\}_{\forall j \in \mathcal{N}(i)}. \tag{5}$$

4 Implementation

4.1 Update Scheme

The single-step update scheme in our model is similar to many fluid simulation methods, which is an advection-projection scheme. In general, given the state (position $\mathbf{x}^n$ and velocity $\mathbf{v}^n$) of the current time step n, we derive the state of next time step $n+1$ by passing the state information through advection net, collision net, and pressure net sequentially (detailed description of update scheme can be found in A.1).

4.2 Network Architectures

We use MLPs as the node update function for the node-focused networks, and we don't use any node update function in the edge-focused network. In the edge-focused network, the edge message

Case	Model	Density error		Velocity divergence		Average Chamfer distance (mm)	
		Mean	Max	Mean	Max	Mean	Max
Dam Collapse	FGN (this work)	0.0461	0.0900	0.0195	0.0280	24.2	30.1
	Ground Truth	0.0380	0.0710	0.0190	0.0268	-	-
Water Fall	FGN (this work)	0.0541	0.1350	0.0207	0.0431	24.8	29.6
	Ground Truth	0.0429	0.0966	0.0196	0.0398	-	-

Table 1: Quantitative accuracy analysis on different metrics (Detailed comparisons against other data-driven models and error trend plot can be found in A.3).

Model	Parameters	Model inference time (ms)	NNS time (ms)
FGN (this work)	**41996**	**5.7**	46.4
GNS	1406272	44.6	33.1
CConv	692902	28.9*	**24.7***
MPS (ground truth)	-	313.2	42.3

Table 2: Runtime analysis of different model. We report the total amount of trainable parameters, the inference time and nearest neighbor searching time in a single frame of each model. The test was carried out on a dam collapse scene containing approximately 40k fluid particles. Note that in CConv, the network and neighbor searching method are based on TensorFlow and Open3D (denoted with *).

function is an MLP that takes edge features as input. In the node-focused network, we calculate the edge messages by calculating a weighted summation of node features on all neighboring nodes (this is similar to using smooth kernel instead of in-degree of nodes as weight function in GCN). A detailed description of message passing function implementation can be found in A.1.

5 Experiments

5.1 Training

We use the Moving Particle Semi-implicit method (MPS) (Koshizuka and Oka, 1996) with an improved pressure solver (Lee et al., 2011) to generate high-fidelity simulation data of incompressible flow. We train three networks, advection net, collision net, and pressure net separately. Each network is trained in a supervised way by optimizing the mean squared error between prediction $\hat{y}$ and ground truth y (See A.2 for full detail of training dataset settings and training strategy). We implement our model with PyTorch and PyTorch Geometric (Fey and Lenssen, 2019).

5.2 Evaluation

We first qualitatively validate our model by visualizing its simulation sequences in testing scenarios [1]. We challenge it with different geometries. Then we measure its position error and several other physics metrics quantitatively. Besides the comparison against ground truth data, we also compare our model to two recent works, graph network simulator (GNS), and continuous convolution (CConv) (Ummenhofer et al., 2020; Sanchez-Gonzalez et al., 2020), which built purely data-driven end-to-end models to simulate fluids under the Lagrangian framework. We benchmark different models in terms of running time (Table 2). In general our model can learn to emulate physic processes involved in fluid dynamics in a computationally efficient way. Although we do not directly supervise on important physics metrics like velocity divergence and particle density distribution , the model gives relatively high-fidelity results in terms of these metrics (Table 1). See A.5 for experiments detail and model generalization to different conditions.

6 Conclusion

In this paper, we present a data-driven Lagrangian fluid model for incompressible fluid simulation by decomposing simulation scheme as separate reasoning tasks based on Navier-Stokes equation. It can preserve many essential physical properties of the fluid field such as low volume compression,

[1] Video link: `https://sites.google.com/view/fluid-graph-network-video/home`

and predict reasonable pressure distribution. Our model also has generalization capability, where it can remain stable when extrapolating to a wide range of different geometries and adopting different time step sizes. In general, our work is an advance in learning on unstructured data with graph neural networks, and enriches the paradigm of combining learning-based methods with physical models as well.

REFERENCES

J. Monaghan, "An introduction to sph," *Computer Physics Communications*, vol. 48, no. 1, pp. 89 – 96, 1988. [Online]. Available: http://www.sciencedirect.com/science/article/pii/0010465588900264

M. Müller, D. Charypar, and M. Gross, "Particle-based fluid simulation for interactive applications," in *Proceedings of the 2003 ACM SIGGRAPH/Eurographics Symposium on Computer Animation*, ser. SCA '03. Goslar, DEU: Eurographics Association, 2003, p. 154–159.

S. Koshizuka and Y. Oka, "Moving-particle semi-implicit method for fragmentation of incompressible fluid," *Nuclear Science and Engineering*, vol. 123, no. 3, pp. 421–434, 1996. [Online]. Available: https://doi.org/10.13182/NSE96-A24205

M. Becker and M. Teschner, "Weakly compressible sph for free surface flows," in *Proceedings of the 2007 ACM SIGGRAPH/Eurographics Symposium on Computer Animation*, ser. SCA '07. Goslar, DEU: Eurographics Association, 2007, p. 209–217.

B. Solenthaler and R. Pajarola, "Predictive-corrective incompressible sph," in *ACM SIGGRAPH 2009 Papers*, ser. SIGGRAPH '09. New York, NY, USA: Association for Computing Machinery, 2009. [Online]. Available: https://doi.org/10.1145/1576246.1531346

J. Bender and D. Koschier, "Divergence-free smoothed particle hydrodynamics," in *Proceedings of the 2015 ACM SIGGRAPH/Eurographics Symposium on Computer Animation*. ACM, 2015.

L. Ladický, S. Jeong, B. Solenthaler, M. Pollefeys, and M. Gross, "Data-driven fluid simulations using regression forests," *ACM Trans. Graph.*, vol. 34, no. 6, Oct. 2015. [Online]. Available: https://doi.org/10.1145/2816795.2818129

J. Tompson, K. Schlachter, P. Sprechmann, and K. Perlin, "Accelerating eulerian fluid simulation with convolutional networks," *CoRR*, vol. abs/1607.03597, 2016. [Online]. Available: http://arxiv.org/abs/1607.03597

X. Xiao, Y. Zhou, H. Wang, and X. Yang, "A novel cnn-based poisson solver for fluid simulation," *IEEE Transactions on Visualization Computer Graphics*, vol. 26, no. 03, pp. 1454–1465, mar 2020.

S. Wiewel, M. Becher, and N. Thuerey, "Latent-space physics: Towards learning the temporal evolution of fluid flow," *CoRR*, vol. abs/1802.10123, 2018. [Online]. Available: http://arxiv.org/abs/1802.10123

J. Morton, A. Jameson, M. J. Kochenderfer, and F. Witherden, "Deep dynamical modeling and control of unsteady fluid flows," in *Advances in Neural Information Processing Systems 31*, S. Bengio, H. Wallach, H. Larochelle, K. Grauman, N. Cesa-Bianchi, and R. Garnett, Eds. Curran Associates, Inc., 2018, pp. 9258–9268. [Online]. Available: http://papers.nips.cc/paper/8138-deep-dynamical-modeling-and-control-of-unsteady-fluid-flows.pdf

F. de Avila Belbute-Peres, T. D. Economon, and J. Z. Kolter, "Combining differentiable pde solvers and graph neural networks for fluid flow prediction," 2020.

F. Scarselli, M. Gori, A. C. Tsoi, M. Hagenbuchner, and G. Monfardini, "The graph neural network model," *IEEE Transactions on Neural Networks*, vol. 20, no. 1, pp. 61–80, 2009.

T. N. Kipf and M. Welling, "Semi-supervised classification with graph convolutional networks," *CoRR*, vol. abs/1609.02907, 2016. [Online]. Available: http://arxiv.org/abs/1609.02907

W. L. Hamilton, R. Ying, and J. Leskovec, "Inductive representation learning on large graphs," 2017.

S. Wang, S. Suo, W.-C. Ma, A. Pokrovsky, and R. Urtasun, "Deep parametric continuous convolutional neural networks," in *Proceedings of the IEEE Conference on Computer Vision and Pattern Recognition (CVPR)*, June 2018.

B. Ummenhofer, L. Prantl, N. Thuerey, and V. Koltun, "Lagrangian fluid simulation with continuous convolutions," in *International Conference on Learning Representations*, 2020.

P. W. Battaglia, R. Pascanu, M. Lai, D. J. Rezende, and K. Kavukcuoglu, "Interaction networks for learning about objects, relations and physics," *CoRR*, vol. abs/1612.00222, 2016. [Online]. Available: http://arxiv.org/abs/1612.00222

M. B. Chang, T. Ullman, A. Torralba, and J. B. Tenenbaum, "A compositional object-based approach to learning physical dynamics," *CoRR*, vol. abs/1612.00341, 2016. [Online]. Available: http://arxiv.org/abs/1612.00341

A. Sanchez-Gonzalez, N. Heess, J. T. Springenberg, J. Merel, M. A. Riedmiller, R. Hadsell, and P. W. Battaglia, "Graph networks as learnable physics engines for inference and control," *CoRR*, vol. abs/1806.01242, 2018. [Online]. Available: http://arxiv.org/abs/1806.01242

Y. Li, J. Wu, R. Tedrake, J. B. Tenenbaum, and A. Torralba, "Learning particle dynamics for manipulating rigid bodies, deformable objects, and fluids," *CoRR*, vol. abs/1810.01566, 2018. [Online]. Available: http://arxiv.org/abs/1810.01566

D. Mrowca, C. Zhuang, E. Wang, N. Haber, L. F. Fei-Fei, J. Tenenbaum, and D. L. Yamins, "Flexible neural representation for physics prediction," in *Advances in Neural Information Processing Systems 31*, S. Bengio, H. Wallach, H. Larochelle, K. Grauman, N. Cesa-Bianchi, and R. Garnett, Eds. Curran Associates, Inc., 2018, pp. 8799–8810. [Online]. Available: http://papers.nips.cc/paper/8096-flexible-neural-representation-for-physics-prediction.pdf

G. K. Batchelor, *An Introduction to Fluid Dynamics*, ser. Cambridge Mathematical Library. Cambridge University Press, 2000.

P. W. Battaglia, J. B. Hamrick, V. Bapst, A. Sanchez-Gonzalez, V. F. Zambaldi, M. Malinowski, A. Tacchetti, D. Raposo, A. Santoro, R. Faulkner, Ç. Gülçehre, H. F. Song, A. J. Ballard, J. Gilmer, G. E. Dahl, A. Vaswani, K. R. Allen, C. Nash, V. Langston, C. Dyer, N. Heess, D. Wierstra, P. Kohli, M. Botvinick, O. Vinyals, Y. Li, and R. Pascanu, "Relational inductive biases, deep learning, and graph networks," *CoRR*, vol. abs/1806.01261, 2018. [Online]. Available: http://arxiv.org/abs/1806.01261

B.-H. Lee, J.-C. Park, M.-H. Kim, and S.-C. Hwang, "Step-by-step improvement of mps method in simulating violent free-surface motions and impact-loads," *Computer Methods in Applied Mechanics and Engineering*, vol. 200, no. 9, pp. 1113 – 1125, 2011. [Online]. Available: http://www.sciencedirect.com/science/article/pii/S0045782510003464

M. Fey and J. E. Lenssen, "Fast graph representation learning with PyTorch Geometric," in *ICLR Workshop on Representation Learning on Graphs and Manifolds*, 2019.

A. Sanchez-Gonzalez, J. Godwin, T. Pfaff, R. Ying, J. Leskovec, and P. W. Battaglia, "Learning to simulate complex physics with graph networks," 2020.

J. L. Ba, J. R. Kiros, and G. E. Hinton, "Layer normalization," 2016.

D. P. Kingma and J. Ba, "Adam: A method for stochastic optimization," 2014.

APPENDIX A

A.1 IMPLEMENTATION DETAILS

Graph construction We build the graph by establishing edges between particles within limit radius. We perform the neighborhood searching on GPU by using cell sort algorithm. All the edge attributes are stored in sparse matrices. Although the limit radius does not have significant impact on training loss and larger limit radius will increase the computing cost drastically, we found that small limit radius can influence the long-term stability of the model. For advection net and pressure projection net, we select the limit radius to be three times the particle diameter D (D = 0.050m), and 0.9D for collision net.

Numerical model In general, we calculate all the gradient operators and field function's value based on numerical model of SPH.

In SPH, an arbitrary scalar (or vector) field $A(\mathbf{r})$ at location $\mathbf{r}$ can be represented by a convolution:

$$A(\mathbf{r}) = \int A(\mathbf{r}') W(|\mathbf{r} - \mathbf{r}'|, h)\, dV(\mathbf{r}'), \tag{6}$$

where W is weighting function or smooth kernel as defined in SPH, h is the smoothing length, which defines the range of particles to be considered and $V(\mathbf{r}')$ is the volume at $\mathbf{r}$. Numerically, the interpolation can be approximated by replacing the integration with a summation.

In SPH model, particle density is defined as:

$$n_i = \sum_{i \neq j} W(|\mathbf{r}_i - \mathbf{r}_j|, h), \forall j \in \mathcal{N}(i). \tag{7}$$

For scalar quantity ϕ_i at location $\mathbf{r}_i$, we approximate its gradient by:

$$\nabla \phi_i = \frac{d}{n^*} \sum_j (\phi_j - \phi_i) \nabla W_{ij}, \tag{8}$$

where n^* is the constant particle number density derived by calculating the maximum particle number density at the initial frame, d is the dimension of the problem, W_{ij} denotes the smooth kernel function value between particle i and j. Similarly velocity divergence is defined as:

$$\nabla \cdot \mathbf{v}_i = \frac{d}{n^*} \sum_j (\mathbf{v}_j - \mathbf{v}_i) \cdot \nabla W_{ij}, \tag{9}$$

We adopt the same smooth kernel function from Koshizuka and Oka (1996), which is very simple to evaluate.

$$W_{ij} = \begin{cases} \frac{h}{||\mathbf{r}_i - \mathbf{r}_j||_2} - 1 & \text{if } ||\mathbf{r}_i - \mathbf{r}_j||_2 < h \\ 0 & \text{if } ||\mathbf{r}_i - \mathbf{r}_j||_2 \geq h \end{cases} \tag{10}$$

Update scheme We update the state of fluid field by passing input to advection net, collision net and pressure net sequentially. The input features to advection net are positions and velocities of particles, $[\mathbf{x}^n, \mathbf{v}^n]$, along with $\mathbf{g}$, which indicates the external body force per mass of fluid, and viscosity parameter ν, which denotes the magnitude of fluid viscosity. The advection net predicts acceleration of particles:

$$\mathbf{a}^{\text{adv}} = G_{\text{adv}}(\mathbf{x}^n, \mathbf{v}^n, \mathbf{g}, \nu), \tag{11}$$

and updates the state of fluid particles to an intermediate state $[\mathbf{x}^*, \mathbf{v}^*]$.

$$\mathbf{v}^* = \mathbf{v}^n + \mathbf{a}^{\text{adv}} \Delta t, \tag{12}$$

$$\mathbf{x}^* = \mathbf{x}^n + \mathbf{v}^* \Delta t. \tag{13}$$

Where $\mathbf{a}^{\text{adv}} = [\mathbf{a}_1^{\text{adv}}, ..., \mathbf{a}_N^{\text{adv}}]$, $\mathbf{x}^n = [\mathbf{x}_1^n, ..., \mathbf{v}_N^n]$, $\mathbf{v}^n = [\mathbf{v}_1^n, ..., \mathbf{v}_N^n]$ for particles $i \in \{1, .., N\}$. We will use the same notation throughout illustration.

The collision net takes relative positions and velocities between particles, $[\mathbf{x}_i^* - \mathbf{x}_j^*, \mathbf{v}_i^* - \mathbf{v}_j^*]$ as input, and predicts correction to the velocity,

$$\Delta \mathbf{v} = G_{\text{col}}(\mathbf{x}_r^*, \mathbf{v}_r^*), \tag{14}$$

where $[\mathbf{x}_r^*, \mathbf{v}_r^*]$ denotes the relative position and velocity in intermediate state. The velocity is then updated with predicted correction:

$$\mathbf{v}^{**} = \mathbf{v}^* + \Delta \mathbf{v}. \tag{15}$$

The updated intermediate position and velocity are taken as input by the pressure net, along with particle number density $\boldsymbol{\rho}$.

$$\hat{\mathbf{p}} = G_{\text{pres}}(\mathbf{x}^*, \mathbf{v}^{**}, \boldsymbol{\rho}). \tag{16}$$

The state of fluid field is then updated to next time step $n+1$,

$$\mathbf{v}^{n+1} = \mathbf{v}^{**} - \frac{\nabla \hat{\mathbf{p}}}{\rho_c} \Delta t, \tag{17}$$

$$\mathbf{x}^{n+1} = \mathbf{x}^* + \mathbf{v}^{n+1} \Delta t. \tag{18}$$

Where $\hat{\mathbf{p}} = [\hat{p}_1, ..., \hat{p}_N]$, $\boldsymbol{\rho} = [\rho_1, ..., \rho_N]$, ρ_c is the density parameter of fluid. Predicting pressure of fluid field using particle density and velocity is based on the observation that advection will incur a temporary compression on fluid body, which means fluid density has changed. Therefore the goal of pressure net is to impose a pressure projection to mitigate these deviations.

During the above calculation, the global positional information is only used to construct graph on fluid particles and will not be passed into aggregator and processor as features. The relative position and particle density are normalized before input.

Message passing function For node-focused graph network, to derive a smooth response of the field with respect to spatial location, the edge message passing, aggregation and node update from layer $l-1$ to l is defined as:

$$\mathbf{a}_i^{(l)} = \frac{\sum \mathbf{f}_j^{(l-1)} W\left(\left|\mathbf{r}_i - \mathbf{r}_j\right|, h\right)}{\sum W\left(\left|\mathbf{r}_i - \mathbf{r}_j\right|, h\right)} + \mathbf{f}_i^{(l-1)}, \forall j \in \mathcal{N}(i), \tag{19}$$

$$\mathbf{f}_i^{(l)} = \sigma\left(\mathbf{W} \cdot \mathbf{a}_i^{(l)}\right), \tag{20}$$

where the aggregator sums up the features $\mathbf{f}_j^{(l-1)}$ from neighbor vertices $\{v_j | j \in \mathcal{N}(i)\}$ using smooth kernel as weight function, and here self-connection is added to every vertex. Linear transformation $\mathbf{W}$ and non-linear transformation σ are then applied to the aggregated features. In practice we found that two layers of message passing plus a MLP processor which takes node embedding output from previous layer as input is enough for the model to produce reasonably accurate output (Adding more aggregation layers does not bring in significant improvements).

For edge-focused network, we do not define any node update, where we only do update on edges and aggregate them to nodes in the final layer. the edge message function is a MLP, Θ, which takes edge features as input.

$$\mathbf{r}_{ji} = \Theta(\mathbf{e}_{ji}), \tag{21}$$

As for the edge-focused The aggregation in the last layer is simply defined as:

$$\mathbf{a}_i = \sum_{j \in \mathcal{N}(i)} \mathbf{W} \cdot \mathbf{r}_{ji}, \tag{22}$$

where $\mathbf{r}_{ji}$ is edge feature processed by processor, $\mathbf{W}$ is a linear transformation matrix. The aggregation in the edge-focused network is at the last layer, so no non-linearity is included here.

The processors in both networks are implemented as shared MLP, where they are shared among nodes or edges depending on network types (e.g. in the node-focused network, the processor is a MLP shared among each node). In a node-focused network, the processor has three hidden layers, with the input node embedding $\mathbf{f}$ of size 128. In an edge-focused network, the processor has four hidden layers, with input edge attributes $[\mathbf{x}_r, \mathbf{v}_r]$ of size 6.

A.2 TRAINING

Dataset Generation We use MPS to generate ground truth and reference sequence. MPS is a numerical method based on SPH which prioritizes accuracy over calculation speed. It enforces the incompressibility of the fluid field by solving the pressure Poisson equation. We created 20 scenes by randomly placing fluid blocks, solid obstacles, initializing fluid particles with random velocity We place one or two of the following basic obstacles (as shown in Figure 2) in training scenes. In addition to obstacles, each scene is a cubic box (80x80x40) containing a fluid block (25x25x10) (as shown in Figure 2). We place the fluid block at random place in the box and initialize its velocity of one direction by uniformly sampling from $\mathcal{U}(0, 0.1)$. We generated 20 scenes adopting above settings and simulate each training scene to 1000 time steps with step size $dt = 0.002$.

Strategy We use mean squared error to measure the distance between ground truth and model prediction.

$$L = \frac{1}{N}\sum_{i=1}^{N}||y_i - \hat{y}_i||_2^2 \tag{23}$$

We normalize particle density before inputting into the pressure net, which accelerates and stabilizes training. In the processor, we add LayerNorm (Ba et al., 2016) after activation to each layer (except for the output layer). The parameters of the model are optimized with Adam (Kingma and Ba, 2014) optimizer. We implement the model in PyTorch. All the training and experiments are mainly carried out on NVIDIA GTX 1080Ti GPU.

In each time step of the ground truth simulator, there are mainly three steps. First, advect fluids with body force and viscosity:

$$\mathbf{v}^* = \mathbf{v}^n + \mathbf{a}^{\text{adv}}\Delta t, \tag{24}$$

$$\mathbf{x}^* = \mathbf{x}^n + \mathbf{v}^*\Delta t, \tag{25}$$

and then solve the pressure poisson equation,

$$\nabla^2 p = \frac{1}{\Delta t}\nabla \cdot \mathbf{v}^*, \tag{26}$$

lastly,

$$\mathbf{v}^{n+1} = \mathbf{v}^* - \frac{\nabla p}{\rho_c}\Delta t, \tag{27}$$

$$\mathbf{x}^{n+1} = \mathbf{x}^* + \mathbf{v}^{n+1}\Delta t. \tag{28}$$

Here, we use $[\mathbf{x}^*, \mathbf{v}^*, \mathbf{g}, \nu]$ as the training features and $\mathbf{a}^*$ (i.e. $(\mathbf{v}^* - \mathbf{v}^n)/\Delta t$) as the training label for advection net. $[\mathbf{x}^*, \mathbf{v}^*]$ and particle density $\boldsymbol{\rho}$ (evaluated based on $\mathbf{x}^*$) are the training features for pressure net, with pressure p as label. To train collision net, we simulate another particle system that is updated only based on elastic collision rule and applies no other dynamics. We use relative velocity and position before collision as inputs, and use velocity difference (i.e. Δv) as output target.

We train each network for 100,000 iterations of gradient updates and decay learning rate from 0.001 to 0.0000625. For the training of three sub-networks (advection net, collision net, pressure net), the batch size of each network is 16, 4 and 32 respectively. To allow the mini-batching of different graph, we mini-batch the adjacency matrix of different scenes by creating a large sparse matrix and stacking adjacency matrix on the diagonals.

A.3 METRICS EVALUATION DETAILS

In the experiments, we first measure our model's prediction against ground truth solver. We also include comparison with two purely data-driven models, Graph Network Simulator and Continuous Convolution, which are end-to-end deep learning models using little physic priors. Ummenhofer et al. (2020) use the continuous convolutional kernel to learn fluid dynamics and they reported that their model has outperformed other similar works in this domain. Sanchez-Gonzalez et al. (2020) propose a graph network-based simulator (GNS) as a general-purpose physic simulator under Lagrangian representation. Our model and GNS both transform and pass messages of fluid field via graph structures, but GNS consists of a far larger and deeper network with multiple sub-blocks and thus contains much more parameters than ours. For all baseline models, we adopt the same training strategy from original papers but train them on our dataset.

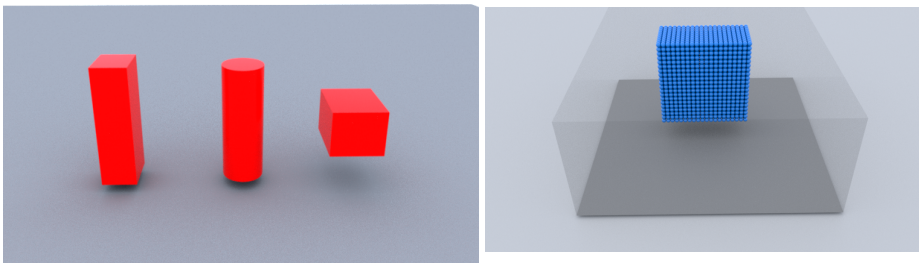

(a) Obstacles: Square pillar, cylinder and cube

(b) Fluid block and box

Figure 2: Visualizations of training settings

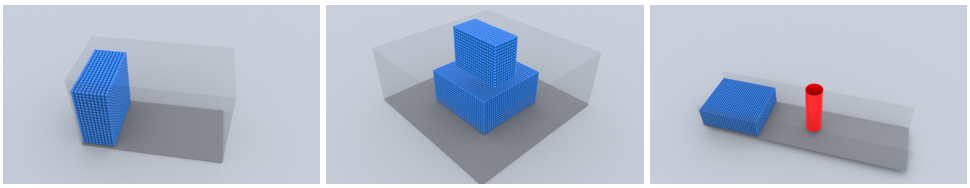

(a) Dam Collapse

(b) Water Fall

(c) Flow around Cylinder

Figure 3: Visualizations of initial condition settings in evaluation scenarios

Metrics To conduct quantitative analysis, we evaluate model performance based on several metrics. We report the asymmetric version of Chamfer Distance between the simulated results of different models and ground truth sequence. The asymmetric Chamfer distance for two collections of particles X, Y (from X to Y) is defined as:

$$L\left(X, Y\right) = \frac{1}{N} \sum_{\mathbf{x} \in X} \min_{\mathbf{y} \in Y} d\left(\mathbf{x}, \mathbf{y}\right), \tag{29}$$

where N is the total particle number of point cloud collection X, and distance function $d(\mathbf{x}, \mathbf{y})$ is evaluated using L2-norm $\|\mathbf{x}-\mathbf{y}\|_2$. We investigate two essential physical quantities for incompressible fluid simulation - velocity divergence and particle density deviation of fluid field. In addition, we use normalized mean absolute error (MAE) and relative tolerance to evaluate the error of advection net and pressure net on single frame inference respectively. The normalized MAE from prediction $\hat{y}$ to ground truth y is defined as:

$$L_{\text{MAE}} = \frac{1}{N} \sum \frac{|\hat{y} - y|}{|y|}. \tag{30}$$

The relative tolerance of the numerical solution $\hat{\mathbf{x}}$ to a linear system $A\mathbf{x} = \mathbf{b}$ can be defined as:

$$tol = \frac{||A\hat{\mathbf{x}} - \mathbf{b}||_2}{||\mathbf{b}||_2}. \tag{31}$$

Results We show the error trend of dam collapse and water fall scene under different evaluation metrics in Figure 4. The quantitative analysis is reported at Table 3 The position error trend of different time step sizes is shown in Figure 5. Qualitative results of pressure prediction are shown in Figure 6.

In addition, we study the performance of each sub-network in our model as stand-alone solvers for sub-dynamical systems and report their relative error in Table 4. For the advection net, we challenge it by applying a different set of material parameters (i.e. different gravity and viscosity parameters). We report the normalized mean absolute error (MAE) between prediction and ground truth.

$$L = \frac{1}{N} \sum \frac{|\dot{\mathbf{u}}_{\text{pred}} - \dot{\mathbf{u}}_{\text{gt}}|}{||\dot{\mathbf{u}}_{\text{gt}}||_2}. \tag{32}$$

For pressure net, we evaluate the relative tolerance of its predicted solution $\hat{\mathbf{p}}$ to the discretized pressure poisson equation (i.e. $A\mathbf{p} = \mathbf{b}$). The relative low error demonstrates the capability of our sub-networks in learning and emulating different dynamical systems.

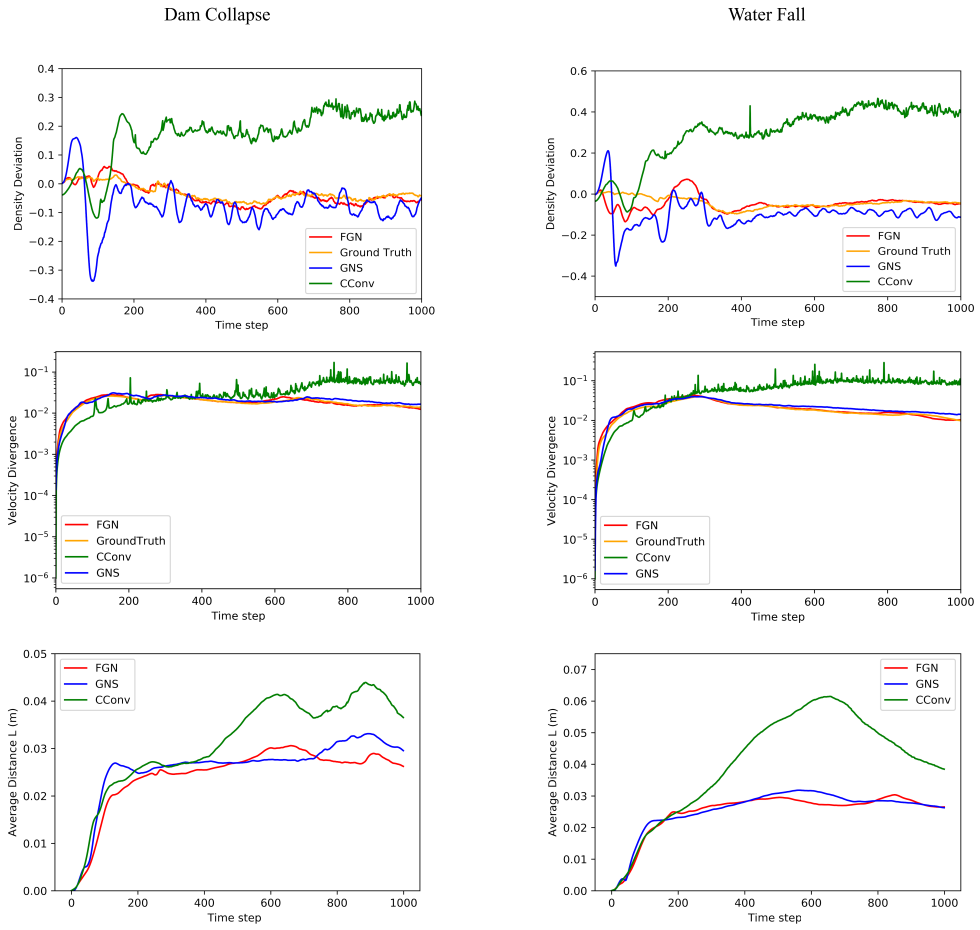

Figure 4: Error trend with respect to time. The density deviation of our model remain close to zero despite some oscillation at first. Although GNS also maintains a low density deviation, its average density oscillates more severely. This is consistent with the qualitative comparison, in which the fluid surface from GNS is oscillating and less compact. CConv fails to maintain constant density and its density increases significantly after collision to the wall boundary. Both our model and GNS can predict a low divergence velocity field while CConv fails to capture this property. This somehow explains why CConv struggles to maintain constant density.The average Chamfer distance to the ground truth data accumulates at first and stabilizes after system is in equilibrium. CConv has larger average Chamfer distance while graph-based model's distances are smaller.

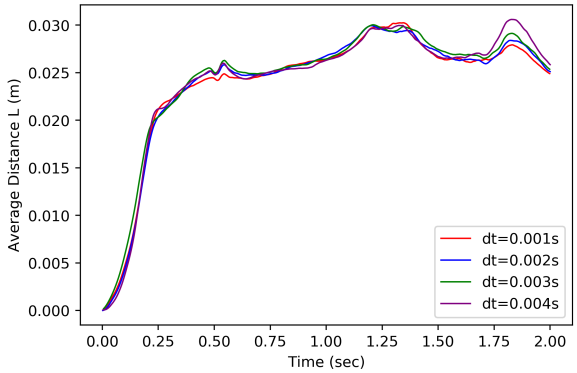

Figure 5: Average Chamfer distance to the ground truth data of FGN model under different time step sizes. FGN can generalized to different time scale with minor difference in performance. The training data uses a time step size of $dt = 0.002s$, and FGN converges for all $dt < 0.005s$.

Case	Model	Density error		Velocity divergence		Average Chamfer distance (mm)	
		Mean	Max	Mean	Max	Mean	Max
Dam Collapse	FGN (this work)	**0.0461**	**0.0900**	**0.0195**	**0.0280**	**24.2**	**30.1**
	GNS	0.0898	0.3387	0.0210	0.0311	26.1	33.1
	CConv	0.1811	0.2947	0.0338	0.1700	31.4	44.0
	Ground Truth	0.0380	0.0710	0.0190	0.0268	-	-
Water Fall	FGN (this work)	**0.0541**	**0.1350**	**0.0207**	**0.0431**	**24.8**	**29.6**
	GNS	0.1035	0.3512	0.0223	**0.0399**	25.6	31.8
	CConv	0.2783	0.4121	0.0668	0.2882	40.4	61.5
	Ground Truth	0.0429	0.0966	0.0196	0.0398	-	-

Table 3: Quantitative accuracy analysis. For resolution, the dam collapse case contains about 10k particles and water fall case contains about 80k particles. We report the mean and maximum value of density error and velocity divergence over the whole simulation sequence. We also report the average Chamfer distance between the results of each model and ground truth data.

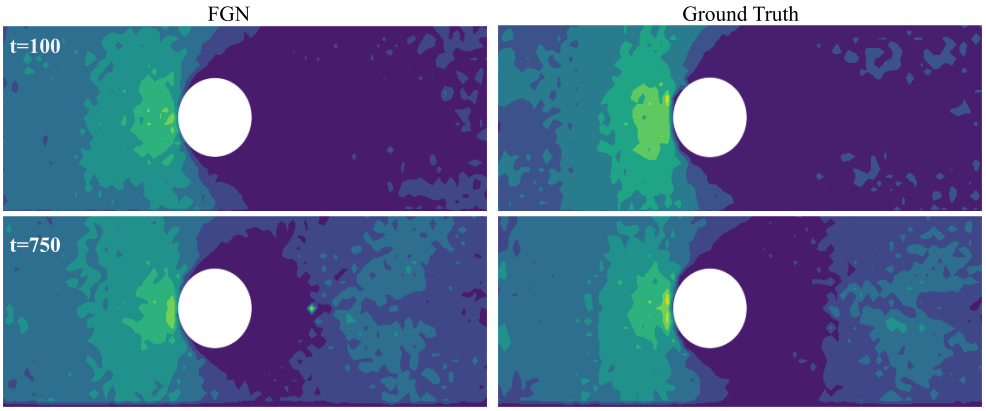

Figure 6: Pressure distribution contour. Our model can learn to generate reasonable pressure distribution. The distribution agreed with ground truth, which captures the shape of shifting high pressure and low pressure region.

Model	Dynamical system	Model Output	Evaluation metric	Error
Advection Net	$\dot{\mathbf{u}} = \mathbf{g} + \nu\nabla^2\mathbf{u}$	prediction of $\dot{\mathbf{u}}$	Normalized MAE	$12.4\% \pm 5.6\%$
Pressure Net	$\nabla^2 p = \frac{1}{\Delta t}\nabla \cdot \mathbf{u}^*$	prediction of p	Relative tolerance	$8.3\% \pm 1.1\%$

Table 4: Quantitative analysis of advection net and pressure net. We evaluate advection net's performance as solver for a forward problem. We generate ten sequences with different set of material parameters as test data for advection net. The gravity $\mathbf{g}$ for test data ranges from 1.0 to 100.0 and viscosity parameter ν ranges from 0.1 to 0.0001. For pressure net, we report its error as solver for a linear equation system.

Case	Model	Density error		Velocity divergence		Average Chamfer distance (mm)	
		Mean	Max	Mean	Max	Mean	Max
Dam Collapse	FGN (this work)	**0.0461**	**0.0900**	**0.0195**	**0.0280**	**24.2**	**30.1**
	GCN	0.0939	0.3832	0.0196	0.0293	27.7	31.6
	SAGE	0.0935	0.3597	0.0196	0.0289	26.4	31.3
	MLP	0.0963	0.3624	0.0196	0.0289	28.5	32.8
	Ground Truth	0.0380	0.0710	0.0190	0.0268	-	-
Water Fall	FGN (this work)	**0.0541**	**0.1350**	**0.0207**	**0.0431**	**24.8**	**29.6**
	GCN	0.0794	0.3373	0.0210	0.0433	25.5	31.7
	SAGE	0.0769	0.3254	0.0209	0.0432	25.3	31.4
	MLP	0.0830	0.2967	0.0209	0.0433	26.3	32.4
	Ground Truth	0.0429	0.0966	0.0196	0.0398	-	-

Table 5: Quantitative ablation study. We compare our aggregator against graph convolution networks (GCN) from Kipf and Welling (2016), Hamilton et al. (2017)'s graph SAGE using mean aggregator and MLP *w/o* any graph aggregation operation. All aggregators have two layers.

A.4 Ablation Study Details

Performance of different message passing and aggregation mechanisms is listed in Table 5.

A.5 Baselines Implementation

Continuous Convolution We use the open-source implementation from Ummenhofer et al. (2020) [2]. To give a fair benchmark result we train their network with our dataset. Note our training dataset is much smaller than theirs and does not include complex geometries. As in our work, we model solid obstacles and wall as virtual particles, so we transform these virtual particles into surface and corresponding normals before inputting them into CConv network. The original CConv uses a time step size of 0.02s, but given such a large time step size, the qualitative results can be distinct from ground truth and other model with smaller time step size. Hence during training and comparison we adopt a time step size of 0.002s for CConv model.

Graph Network-based Simulator We implemented GNS following the description in Sanchez-Gonzalez et al. (2020). We build GNS with 10 unshared GN blocks, conditioned on 5 previous velocities and input relative positions as edge features. We chose the connectivity radius to be 2.1D, so that the number of neighbors is around 20. Sanchez-Gonzalez et al. (2020) use finite-difference to calculate acceleration and velocity, but in our implementation, we explicitly maintain an array to store the velocities of all particles. Additionally, we do not use learned embedding but simple zero and one to indicate particle material type, as in our testing domain there are only two kinds of particles - solid and fluid. The loss function and training procedure are implemented as described in Sanchez-Gonzalez et al. (2020), including noise injection and similar normalization techniques.

For the implementation of GN block, as Sanchez-Gonzalez et al. (2020) states "We use GNs without global features or global updates (similar to an interaction network)", so we implement the GN block update mechanism following the description in Battaglia et al. (2018).

$$\mathbf{e}'_k = \phi^e(\mathbf{e}_k, \mathbf{v}_{r_k}, \mathbf{v}_{s_k}, \mathbf{u}) \tag{33}$$

$$\mathbf{v}'_i = \phi^v(\hat{\mathbf{e}}'_k, \mathbf{v}_i, \mathbf{u}) \tag{34}$$

$$\hat{\mathbf{e}}'_i = \rho^{e\to v}\left(E'_i\right) \tag{35}$$

where ϕ is the update function and implemented as MLP here, ρ is aggregation function which aggregates all the edge attributes to its center vertex, $\mathbf{u}$ is the global feature and here we append them to the nodal features as input feature, r_k denotes receiver vertices and s_k denotes sender vertices.

In the testing stage, as authors did not state how to set initial velocities, so we just warm start the simulation by calculating the first 5 frames using MPS method and apply GNS to the rest frames.

[2] https://github.com/intel-isl/DeepLagrangianFluids